

Temperature dependence of electronic transitions and optical properties in multiferroic BiFeO₃ nanocrystalline film determined from transmittance spectra

W. W. Li (李文武),¹ J. J. Zhu (诸佳俊),¹ J. D. Wu (吴嘉达),² J. Gan (干洁),² Z. G. Hu (胡志高),^{1,a)} M. Zhu (朱敏),³ and J. H. Chu (褚君浩)¹

¹Key Laboratory of Polar Materials and Devices, Ministry of Education, Department of Electronic Engineering, East China Normal University, Shanghai 200241, People's Republic of China

²Key Laboratory for Advanced Photonic Materials and Devices, Ministry of Education, Department of Optical Science and Engineering, Fudan University, Shanghai 200433, People's Republic of China

³Department of Physics, Shanghai Jiao Tong University, Shanghai 200240, People's Republic of China

(Received 11 August 2010; accepted 26 August 2010; published online 21 September 2010)

The ultraviolet-infrared transmittance spectra of BiFeO₃ nanocrystalline film have been studied in the temperature range 5.3–300 K. A redshift trend of the absorption edge and optical constants with increasing the temperature can be observed. Four interband electronic transitions can be uniquely assigned and strongly depend on the temperature. Moreover, two magnetic transitions located at about 150 and 200 K have been observed and can be interpreted as spin-reorientation transitions. It was found that the optical band gap decreases from 2.69 ± 0.01 to 2.65 ± 0.01 eV with increasing the temperature due to the modification of the electron-phonon interactions. © 2010 American Institute of Physics. [doi:10.1063/1.3489926]

Multiferroic materials have attracted much attention due to the coexistence of ferroelectricity and ferromagnetism (or antiferromagnetism). The ability to couple to either the electric or the magnetic polarization allows an additional degree of freedom in device design such as information storage devices and magnetic sensors.^{1–3} In particular, BiFeO₃ (BFO) is known to be the only material that is both ferroelectric ($T_C \sim 1100$ K) and antiferromagnetism ($T_N \sim 640$ K) at room temperature (RT).¹ Furthermore, BFO displays many exotic properties including magnetoelectric coupling, a large polarization, and photovoltaic current.⁴ These advantages make BFO an interesting multiferroic material for the exciting applications in polar oxide-based solar cells and actuators, and multiply controlled devices. Owing to the small mismatch between the film and substrate, BFO films grown on (111)-SrTiO₃ (STO) substrate exhibit the (111)-preferential orientation and a giant polarization ($\sim 100 \mu\text{C}/\text{cm}^2$) along the principal (111) polarization direction.⁵

Up to date, the diverse optical constants and optical band gap (OBG) of BFO films at RT have been reported by different groups.^{6–8} Recent experimental observations revealed some optical excitations at RT because of the hybridization and/or transfer among the Fe, Bi, and O states.^{8,9} However, the intrinsic mechanisms of the optical features and its temperature evolution are less presented. Note that temperature dependence of the OBG energy from the interband transitions can provide important information about the electron-phonon interactions and collective excitations.¹⁰ In this letter, the optical properties of BFO film on STO (111) substrate and the temperature dependence have been investigated by spectral transmittance technique.

Nanocrystalline BFO film with the nominal thickness of about 330 nm was prepared on STO (111) substrate by pulsed laser deposition.^{11,12} The crystalline structure of the BFO film was analyzed by x-ray diffraction (XRD). Far-

infrared (FIR) reflectance spectra were measured using a Bruker VERTEX 80 V Fourier transform infrared spectrometer. Raman spectra were collected by a micro-Raman spectrometer. The normal-incident transmittance spectra were recorded using a double beam ultraviolet-infrared spectrophotometer (PerkinElmer Lambda 950) at the photon energy from 0.5 to 6.5 eV. The BFO film and STO substrate at 5.3–300 K were mounted into an optical cryostat (Janis SHI-4–1) for variable temperature experiments, respectively.

Figure 1(a) shows the XRD pattern of the BFO film and there is no impurity phase. The film is well crystallized with the rhombohedral phase and presents a (111) single crystal-line orientation. The FIR reflectance spectrum in Fig. 1(b) is similar to that from BFO single crystal, which indicates that the film is of high crystalline quality.¹³ Compared to the STO substrate, six $E_1(\text{TO})$ vibration modes can be observed. Raman scattering spectrum in Fig. 1(c) indicates that the three intense peaks at 75 cm^{-1} , 137 cm^{-1} , and 167 cm^{-1} can be assigned to $E(\text{TO}1)$, $A_1(\text{TO}1)$, and $A_1(\text{TO}2)$, respectively. These values are slightly less than that from the films deposited on STO (001) substrates.¹⁴ The five phonon modes lo-

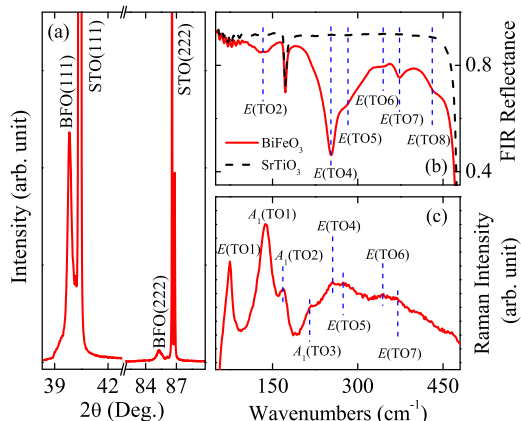


FIG. 1. (Color online) (a) The XRD patterns, (b) far-infrared reflectance spectra, and (c) Raman scattering spectra of the BiFeO₃ film.

^{a)}Author to whom correspondence should be addressed. Electronic mail: zghu@ee.ecnu.edu.cn. Tel.: +86-21-54345150. FAX: +86-21-54345119.

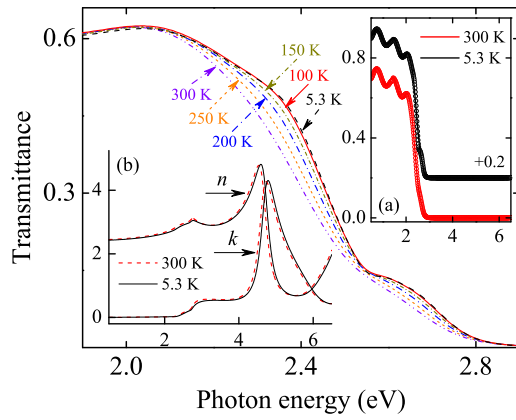


FIG. 2. (Color online) The enlarged band gap region of the BiFeO₃ film at temperatures of 300 K, 250 K, 200 K, 150 K, 100 K, and 5.3 K, respectively. Inset (a) shows the experimental (dotted curves) and fitting (solid curves) transmittance spectra. Inset (b) shows the optical constants n and k .

cated at higher frequencies are $A_1(\text{TO}3)$, $E(\text{TO}4)$, $E(\text{TO}5)$, $E(\text{TO}6)$, and $E(\text{TO}7)$, respectively.¹⁵

A three-phase layered structure (air/film/substrate) was constructed to simulate the transmittance spectra of the BFO film. The normal-incident transmittance spectra cannot be sensitive to the thinner surface rough layer, which could be several nanometers and much less than the film thickness. Therefore, the surface rough layer can be reasonably neglected owing to a slight contribution in the evaluation of the optical properties. The optical constants of the BFO film can be expressed using four Tauc–Lorentz (TL) oscillators.¹⁶ As an example, the experimental and fitting transmittance spectra of the BFO film at 300 K and 5.3 K are shown in the inset (a) of Fig. 2 with the dotted and solid curves, respectively. From Fig. 2, it can be observed that the absorption edge remarkably shift toward the lower energy with increasing the temperature, suggesting that the OBG of the film has a negative temperature coefficient. Especially, two broadening shoulder structures appear and the intensities become much stronger with decreasing the temperature.

For a comparison, the TL parameter values of the BFO film at 300 and 5.3 K are listed in Table I. As can be seen in Table I, four optical transition peaks at RT are located at 2.27 ± 0.01 eV, 2.72 ± 0.02 eV, 4.65 ± 0.01 eV, and 6.90 ± 0.03 eV, respectively. Based on the theoretical calculations and experimental observations, the four energy bands can be uniquely assigned to the following electronic transitions: (1) on-site Fe³⁺ d to d crystal field transition; (2) majority channel Fe $3d$ to O $2p$ charge transfer excitation; (3)

TABLE I. The Tauc–Lorentz parameter values of the BiFeO₃ film at 300 and 5.3 K. Note that the thickness is estimated to 331 ± 1 nm and the ϵ_∞ is 1.74 ± 0.01 for the film measured at different temperature. A , E_p , Γ , and E_0 is the amplitude, peak position energy, broadening term, and Tauc gap energy of the oscillator, respectively.

Temperature (K)	Oscillator	A	E_p (eV)	Γ (eV)	E_0 (eV)
300	TL1	90.4 ± 0.4	2.27 ± 0.01	1.38 ± 0.01	2.21 ± 0.01
	TL2	167 ± 1	2.72 ± 0.02	0.23 ± 0.01	2.68 ± 0.01
	TL3	11.1 ± 0.1	4.65 ± 0.01	0.35 ± 0.01	0.11 ± 0.01
	TL4	4.70 ± 0.02	6.90 ± 0.03	0.13 ± 0.01	0.32 ± 0.01
5.3	TL1	90.9 ± 0.1	2.31 ± 0.01	1.37 ± 0.01	2.27 ± 0.01
	TL2	167 ± 1	2.70 ± 0.01	0.23 ± 0.01	2.69 ± 0.01
	TL3	11.1 ± 0.1	4.70 ± 0.01	0.34 ± 0.01	0.10 ± 0.01
	TL4	4.70 ± 0.01	6.94 ± 0.01	0.13 ± 0.01	0.32 ± 0.01

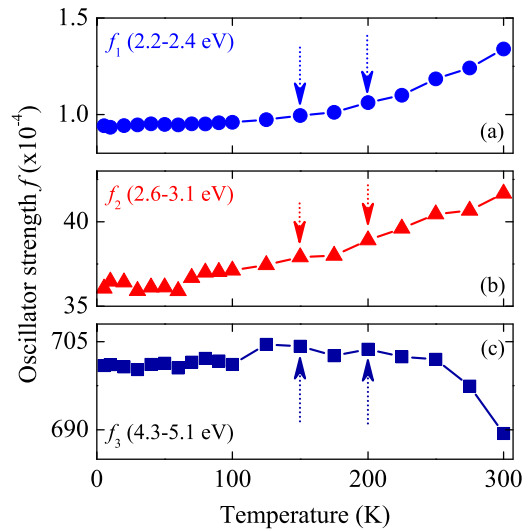


FIG. 3. (Color online) The oscillator strength of the first three electronic excitations as a function of temperature from 5.3 to 300 K. The dashed arrows indicate the magnetic transitions at temperatures of 150 K and 200 K, respectively.

minority channel dipole-allowed O p to Fe d charge transfer excitation; and (4) strong hybridized majority channel O p and Fe d to Bi p state excitation, respectively.^{4,9,17–19} Within the experimental error bars, the energy positions shift toward the higher energy at the temperature of 5.3 K except for the second excitation, which can be attributed to the energy band variations. Under the influence of the tetrahedral crystal field, the Fe $3d$ orbital states split into t_{2g} and e_g state and the t_{2g} state strongly hybridized with the O p orbital.⁴ With decreasing the temperature, the t_{2g} and e_g states can be located at different level in the energy space, which can affect the electronic excited ability of the Bi, Fe, and O states. On the other hand, the evaluated optical constants of the BFO film is presented in Fig. 2(b).

The oscillator strength f can be calculated using the partial sum rule: $f = 2c / (N_e \hbar \pi \omega_p^2) \int_{E_1}^{E_2} n \alpha dE$.⁹ Figure 3 shows the f curves of the first three electronic transitions in the temperature range from 5.3 to 300 K. From Figs. 3(a) and 3(b), the f_1 and f_2 values are kept as a constant at the low temperature region while strikingly increase with further increasing the temperature. This is because the structure distortion and spin-orbit coupling relaxes the spin selection rule with decreasing the temperature. The excitations, which benefit from hybridization and are assisted by vibronic interactions involving odd-parity phonons, can further affect the oscillator strength.⁹ However, the f_3 value is decreased at higher temperature. Note that two small peaks at 150 and 200 K can be observed from the f curves, which are associated with magnetic transitions. The anomalies have been found from Raman experiment results (about 140 and 201 K) and interpreted as spin-reorientation (coupled magnetoelastically to strain) transitions.^{18–20} With decreasing the temperature, the spins rotate out of a plane at 200 K and become orthogonal to the plane at 150 K.²⁰ Through the antisymmetric component of superexchange interaction, the Fe $3d$ magnetic moment couple to the oxygen atoms results in a weak ferromagnetic moment. The magnetic anisotropy is temperature dependent and results in a spontaneous rotation of the ordered spins within a certain temperature interval.²¹ In addition, the spin glass behavior at low temperatures with the

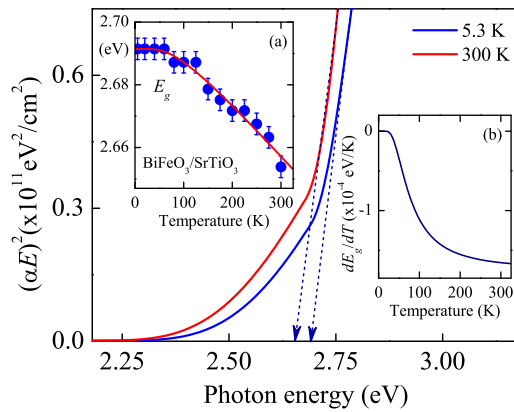


FIG. 4. (Color online) Variations in $(\alpha E)^2$ with the photon energy E are used to determine the OBG E_g of the BiFeO₃ film at temperatures of 300 K and 5.3 K, respectively. Inset (a) shows the temperature dependence of the E_g (dotted curve) and Bose–Einstein model fitting result (solid curve). Inset (b) shows the band gap narrowing coefficient.

competition between ferromagnetic and antiferromagnetic ordering could be another cause for the transition at 200 K.²²

The power law behavior of Tauc $(\alpha E)^2 \propto (E - E_g)$ is for allowed direct transition, here α is the absorption coefficient, E is the incident photon energy, and E_g is the OBG energy.¹⁰ From Fig. 4, it can be found that the OBG value increases from 2.65 ± 0.01 to 2.69 ± 0.01 eV, corresponding to decreasing the temperature from 300 to 5.3 K. Note that the OBG value at RT is less than that prepared on DyScO₃ substrate (2.75 eV) and previous theoretical prediction 2.8 eV.^{23,24} Note further that the overall redshift value of the OBG is larger than that reported on BFO films by Basu *et al.*¹⁷ (28 meV) while less than that from Bi_{3.25}La_{0.75}Ti₃O₁₂ film (50 meV).¹⁰ The observed decrease in the E_g with the temperature can be described using the Bose–Einstein model. From Fig. 4(a), the fitting result indicates that the OBG energy toward 0 K $E_g(0)$ value is about 2.69 ± 0.01 eV. The strength of the electron phonon interaction a_B and the characteristic temperature representing the effective phonon on the temperature scale Θ_B are 21 meV and 238 K, respectively. It is widely recognized that the electron-phonon interaction and the lattice thermal expansion are responsible for the shrinkage in the OBG with the temperature.²⁵ In particular, the electron-phonon interaction, which includes the contributions from both acoustic as well as optical phonons, is usually the dominating one. With increasing the temperature, the longitudinal phonons change the interatomic distance along the direction of their propagation, the transversal modes those perpendicular to their propagation.²⁶ Therefore, the lattice constant of the BFO film maybe change due to the dilatation of lattice and the shortening of interatomic distances. The variation in the lattice constant results in the modification of energy band structure, which further move the conduction band downward and the valence band upward.^{27,28} The band gap narrowing coefficient of the BFO film obtained by the formula $\beta = dE_g/dT$ is plotted in the inset of Fig. 4(b). The coefficient is calculated to be about -1.65×10^{-4} eV/K at RT and less than that from Bi_{3.25}La_{0.75}Ti₃O₁₂ film (-2.65×10^{-4} eV/K).¹⁰

In summary, the detailed temperature effects on the electronic transitions, optical constants, and magnetic transitions of multiferroic BFO film have been investigated using ultraviolet-infrared transmittance spectra.

We acknowledge Dr. Zhijun Qiu at Fudan University for Raman experiments. This work was supported by NSFC (Grant No. 60906046), “973” Program (Grant Nos. 2007CB924901 and 2011CB922200), MOE Program (Grant No. NCET-08-0192), and SMCST Projects (Grant Nos. 10DJ1400201, 08JC1409000, 08520706100, and 09ZZ42).

- ¹J. Wang, J. B. Neaton, H. Zheng, V. Nagarajan, S. B. Ogale, B. Liu, D. Viehland, V. Vaithyanathan, D. G. Schlom, U. V. Waghmare, N. A. Spaldin, K. M. Rabe, M. Wuttig, and R. Ramesh, *Science* **299**, 1719 (2003).
- ²G. Catalan and J. F. Scott, *Adv. Mater.* **21**, 2463 (2009).
- ³N. A. Hill, *J. Phys. Chem. B* **104**, 6694 (2000).
- ⁴P. Chen, N. J. Podraza, X. S. Xu, A. Melville, E. Vlahos, V. Gopalan, R. Ramesh, D. G. Schlom, and J. L. Musfeldt, *Appl. Phys. Lett.* **96**, 131907 (2010).
- ⁵M. K. Singh, H. M. Jang, S. Ryu, and M. H. Jo, *Appl. Phys. Lett.* **88**, 042907 (2006).
- ⁶A. Kumar, R. C. Rai, N. J. Podraza, S. Denev, M. Ramirez, Y. H. Chu, L. W. Martin, J. Ihlefeld, T. Heeg, J. Schubert, D. G. Schlom, J. Orenstein, R. Ramesh, R. W. Collins, J. L. Musfeldt, and V. Gopalan, *Appl. Phys. Lett.* **92**, 121915 (2008).
- ⁷J. Allibe, K. Bougot-Robin, E. Jacquet, I. C. Infante, S. Fusil, C. Carretéro, J.-L. Reverchon, B. Marcilhac, D. Creteé, J.-C. Mage, A. Barthélémy, and M. Bibes, *Appl. Phys. Lett.* **96**, 182902 (2010).
- ⁸R. V. Pisarev, A. S. Moskvina, A. M. Kalashnikova, and Th. Rasing, *Phys. Rev. B* **79**, 235128 (2009).
- ⁹X. S. Xu, T. V. Brinzari, S. Lee, Y. H. Chu, L. W. Martin, A. Kumar, S. McGill, R. C. Rai, R. Ramesh, V. Gopalan, S. W. Cheong, and J. L. Musfeldt, *Phys. Rev. B* **79**, 134425 (2009).
- ¹⁰Z. G. Hu, Y. W. Li, F. Y. Yue, Z. Q. Zhu, and J. H. Chu, *Appl. Phys. Lett.* **91**, 221903 (2007).
- ¹¹W. W. Li, Z. G. Hu, J. D. Wu, J. Sun, M. Zhu, Z. Q. Zhu, and J. H. Chu, *J. Phys. Chem. C* **113**, 18347 (2009).
- ¹²Y. W. Li, Y. D. Shen, F. Y. Yue, Z. G. Hu, X. M. Ma, and J. H. Chu, *J. Cryst. Growth* **312**, 617 (2010).
- ¹³R. P. S. M. Lobo, R. L. Moreira, D. Lebeugle, and D. Colson, *Phys. Rev. B* **76**, 172105 (2007).
- ¹⁴Y. Yang, J. Y. Sun, K. Zhu, Y. L. Liu, and L. Wan, *J. Appl. Phys.* **103**, 093532 (2008).
- ¹⁵P. Hermet, M. Goffinet, J. Kreisel, and Ph. Ghosez, *Phys. Rev. B* **75**, 220102 (2007).
- ¹⁶G. E. Jellison, Jr. and F. A. Modine, *Appl. Phys. Lett.* **69**, 371 (1996); **69**, 2137 (1996).
- ¹⁷S. R. Basu, L. W. Martin, Y. H. Chu, M. Gajek, R. Ramesh, R. C. Rai, X. Xu, and J. L. Musfeldt, *Appl. Phys. Lett.* **92**, 091905 (2008).
- ¹⁸M. O. Ramirez, A. Kumar, S. A. Denev, N. J. Podraza, X. S. Xu, R. C. Rai, Y. H. Chu, J. Seidel, L. W. Martin, S.-Y. Yang, E. Saiz, J. F. Ihlefeld, S. Lee, J. Klug, S. W. Cheong, M. J. Bedzyk, O. Auciello, D. G. Schlom, R. Ramesh, J. Orenstein, J. L. Musfeldt, and V. Gopalan, *Phys. Rev. B* **79**, 224106 (2009).
- ¹⁹M. O. Ramirez, A. Kumar, S. A. Denev, Y. H. Chu, J. Seidel, L. W. Martin, S.-Y. Yang, R. C. Rai, X. S. Xue, J. F. Ihlefeld, N. J. Podraza, E. Saiz, S. Lee, J. Klug, S. W. Cheong, M. J. Bedzyk, O. Auciello, D. G. Schlom, J. Orenstein, R. Ramesh, J. L. Musfeldt, A. P. Litvinchuk, and V. Gopalan, *Appl. Phys. Lett.* **94**, 161905 (2009).
- ²⁰J. F. Scott, M. K. Singh, and R. S. Katiyar, *J. Phys.: Condens. Matter* **20**, 322203 (2008); **20**, 425223 (2008).
- ²¹P. Rovillain, M. Cazayous, Y. Gallais, A. Sacuto, R. P. S. M. Lobo, D. Lebeugle, and D. Colson, *Phys. Rev. B* **79**, 180411 (2009).
- ²²M. K. Singh, R. S. Katiyar, and J. F. Scott, *J. Phys.: Condens. Matter* **20**, 252203 (2008).
- ²³C. Hincinschi, I. Vrejoiu, M. Friedrich, E. Nikulina, L. Ding, C. Cobet, N. Esser, M. Alexe, D. Rafaja, and D. R. T. Zahn, *J. Appl. Phys.* **107**, 123524 (2010).
- ²⁴S. J. Clark and J. Robertson, *Appl. Phys. Lett.* **90**, 132903 (2007).
- ²⁵S. A. Lourenço, I. F. L. Dias, J. L. Duarte, E. Laureto, E. A. Meneses, J. R. Leite, and I. Mazzaro, *J. Appl. Phys.* **89**, 6159 (2001).
- ²⁶S. Biernacki, U. Scherz, and B. K. Meyer, *Phys. Rev. B* **49**, 4501 (1994).
- ²⁷F. Yakuphanoglu, M. Arslan, M. Küçükislamoğlu, and M. Zengin, *Sol. Energy* **79**, 96 (2005).
- ²⁸B. S. Li, Y. C. Liu, Z. Z. Zhi, D. Z. Shen, Y. M. Liu, J. Y. Zhang, and X. W. Fan, *J. Cryst. Growth* **240**, 479 (2002).